PAPER

Fluorescent Si QD decoration onto a flexible polymeric electrospun nanofibrous mat for the colorimetric sensing of TNT†

Osman Arslan,*[a] Zeynep Aytac[b] and Tamer Uyar*[ab]

UV range light was used for the facile, effective and large-scale synthesis of visible light emitting, surface-protected silicon quantum dots (Si QDs) starting from an amine-functionalized alkoxy silane precursor. Within mild and easy hydrolysis/condensation environments, the use of an amine-functionalized precursor together with a reducing agent resulted in a bright visible green light that could be used for fluorescent analytical detection systems. Visible light emitting Si QDs were investigated and it was found that their emission character depends on the illumination time, hydrolysis/condensation conditions and pretreatments for the silane coupling agents. A Nylon 6,6 electrospun nanofibrous mat was selected as a substrate for decoration by the Si QDs in order to fabricate a flexible and free-standing polymeric nanofibrous mat posessing a visible light emitting character so that it could act as a visible colorimetric sensor. The visible light emitting Si QDs were decorated onto the Nylon 6,6 nanofibrous mats *via* covering the surfaces as a 'nanodress' by a simple impregnation/dip-coating and heat-curing methods. The analytical results revealed that the Si QDs decorated flexible polymeric nanofibrous mats could be utilized for colorimetric trinitrotoluene (TNT) detection in low concentrations.

Introduction

In the previous methods involving silicon precursor reduction reactions, incredibly harsh and highly reductive environments were used for the fabrication of silicon quantum dots (Si QDs).[1–7] These methods include the electrochemical etching of bulk silicon,[1] laser-driven pyrolysis of a silane precursor,[2] specific HF acid treatment,[3] gas phase synthesis under protected conditions,[4] acoustic methods,[5] hydrothermal route[6] and microemulsion synthesis.[7] Additionally, as expected, the above-mentioned fabrication procedures require high temperatures, high pressure, special equipment, extreme conditions, protective gas environments special surface treatments and tedious procedures.[8,9] Therefore, lots of time and chemical precursors are being wasted. In the present study, we performed a facile and mild fabrication route for synthesis

of Si QDs, whereby (3-aminopropyl)triethoxysilane (APTES) was utilized as a silicon source, and a mild reductant played a role under UV light in the formation of the surface-protected Si QDs. Consequently hydrophilic, surface durable, water-dispersible and stable fluorescent Si QDs were obtained. Consequently, a low-cost photochemical strategy providing large quantities with uniform and monodispersed Si QDs was developed with the mentioned reactants for the first time, to the best of our knowledge. Therefore, it can be mentioned that this method may be a candidate for the straightforward fabrication of a large amount of Si QDs. We also found the fluorescent peak was tuneable[10] and the resultant Si QDs could be employed as fluorescent probes for sensing,[11] cell labelling[12] or surface modification applications. Generally, the luminescence features of QD-based nanomaterials is determined by the environmental and surface properties. If the surface and environment of the QDs change, inhomogeneous characteristics can be seen, such as a broadening in the emission. It has been widely shown in investigations that if a QD emitter or fluorophore is embedded or attached/decorated into/onto a matrix, their emission properties can vary. In particular, the surface and physical properties of QD-based emitters must be focused and investigated. From this viewpoint, the origin and characteristics of Si QDs present a highly debated case, especially when their emission properties on different substrates are examined.

As one of the most studied nanofibre production techniques in recent years, electrospinning has been extensively investigated

[a] UNAM-National Nanotechnology Research Center, Bilkent University, 06800, Ankara, Turkey. E-mail: uyar@unam.bilkent.edu.tr, arslan@unam.bilkent.edu.tr

[b] Institute of Materials Science & Nanotechnology, Bilkent University, Ankara, 06800, Turkey

† Electronic supplementary information (ESI) available: XPS, PL measurements, UV measurements, STEM images of the Si QD's, PL deconvolution, high-resolution XPS examinations of the Si QD, SEM observation of the impregnated samples, FT-IR and TGA analysis of the samples, Stern–Volmer plot, acidic and basic resistance, visual observation of the surface complex formation, SEM images of the precipitated SiO_2 with Si QD nanoparticles and sensing comparison of TNT, PNP and toluene. See DOI: 10.1039/c6tc05521d

for the fabrication of ultrafine fibrous structures from polymeric and composites materials.[13] Since the obtained 1D nanofibres exhibit a high surface-area-to-volume and length-to-diameter ratios for diverse applications, it is possible to modify their surfaces with nanoparticles or different molecules for different applications, such as for filtration, sensing or wound dressing.[14,15] In this study, we produced Si QDs and decorated them onto flexible Nylon 6,6 electrospun nanofibrous mats by dip-coating and impregnation methods to investigate their colorimetric sensing properties against TNT as a selective colorimetric sensor.

The most salient impact of this study is that it produced a facile and surface-modified fabrication process for ready-to-use and large-scale Si QDs. Since the fabrication required no extreme conditions and the final material is very valuable, stable, visible light emitting QDs, it is possible to utilize them in different nanoapplications. Especially in this manuscript, it is very clear that we produced very stable, acid–base resistant and visible light emitting nanofibrous electrospun Nylon 6,6 mats deposited with Si QDs. The decorated nanofibres were very stable, morphologically suitable and a proper fit for the optical applications as presented.

Experimental section

Materials

(3-Aminopropyl)triethoxysilane, $C_6H_{17}NO_3Si$ (APTES)) was kindly donated from Evonik Industries (Germany). Nylon 6,6 pellets (relative viscosity: 230.000–280.000), formic acid (98–100%) and sodium ascorbate (99%) were purchased from Sigma-Aldrich. All the chemicals were used as received without any further purification.

Synthesis of surface-protected Si QDs and sensing

For synthesis of the surface-protected Si QDs, APTES was dissolved in water and the reducing agent, sodium ascorbate (99%), was introduced in a 1:4 proportion. The mixture was stirred for 3 min at 500 rpm and placed under UV light (Osram, Ultravitalux, 300 W, radiated power: 315–400 nm (UVA) at 13.6 W, and 280–315 nm (UVB) at 3.0 W, 15 cm length) under constant stirring. After 30, 60 and 90 min UV treatment, aliquots were taken for examination. The UV light source lamp was shut down for 15 min at 30 min intervals for cooling when 60 min and 90 min illumination was applied. The solution was transformed into a pale, red-wine colour and its fluorescence feature was detected immediately. For the sensing experiments, specific concentrations of the TNT were dropped into the Si QDs solution, and the quenching in the fluorescence intensity was measured.

Electrospinning of Nylon 6,6 nanofibres

For the electrospinning of polymeric nanofibres, Nylon 6,6 solution was prepared by dissolving 10% (w/v) Nylon 6,6 pellets in formic acid and then stirring for 3 h at room temperature to obtain a homogeneous and clear solution. The prepared solution was loaded into 10 mL syringes fitted with metallic needles (0.6 mm inner diameter) and then electrospinning was performed by applying 15 kV with a collection distance of 15 cm.

The electrospun Nylon 6,6 nanofibres were collected onto the aluminium foil and then peeled off as a free-standing mat.

Dip-coating and impregnation process

For decoration of the Si QDs onto the Nylon 6,6 nanofibrous mats, 200 microlitre of the Si QDs solution was carefully dropped onto the 2 × 2 cm mats. Since nanofibrous mats have pores, the dropped coating solution was accepted as homogeneous and reached both sides effectively. This method was used as the impregnation route for the surface modification. The surface-decorated mats were dried at both under room conditions for 3 h and at 90 °C for 30 min to observe and optimize the coating process. For the dip-coating process, a home-made set-up was installed and the nanofibrous mat (2 × 2 cm) was withdrawn from the Si QDs solution with 100 mm min^{-1} withdrawal speed. Drying was performed at 90 °C for 30 min. Morphological, structural, fluorescence and sensing experiments were conducted for these Si QDs-decorated nanofibrous mats.

Characterization

The elemental composition investigation (EDX mapping) of the nanofibrous mats before and after the Si QDs decoration was performed together with the morphology and diameter analyses with scanning electron microscopy (SEM) (Quanta 200 FEG, FEI). In order to avoid the electron charging effect, the nanofibrous mats were coated with 5 nm Pt/Au (with PECS-682) prior to the SEM imaging. The average diameters of the nanofibrous mats were calculated by counting and measuring 50–100 fibre diameters and plotting them with respect to their frequencies. Non-linear fitting of the obtained fibre diameters gave an average value with a calculated statistical standard deviation. The surface and elemental composition of the Si QDs, nanofibrous mat and Si QDs-decorated mats were performed by X-ray photoelectron spectroscopy (XPS, Thermo Scientific). XPS spectra were obtained using a flood gun charge neutralizer system equipped with a monochromated Al Kα X-ray source ($h\nu$ = 1486.6 eV) from a 400 mm spot size on the nanofibrous mat. Wide energy survey scans were recorded between 0–1360 eV binding energy range, at a detector pass energy of 200 eV and with an energy step size of 1 eV. High-resolution spectra were obtained at a pass energy of 50 eV and with energy steps of 0.1 eV for each atom.

Additional size, structure, morphological and surface examinations of the Si QDs and nanofibrous mats were conducted by transmission electron microscopy (TEM, Tecnai G2 F30) equipped with an EDS. Detection of the UV-Vis absorption properties of the Si QDs was conducted using a UV-Vis Spectrophotometer (Cary 100). Visible emission features of the synthesized Si QDs and fluorescent probes were detected with a Varian 100 spectrophotometer.

Results and discussion

Si QDs synthesis was performed by the reduction of the APTES with sodium ascorbate in aqueous solution under UV illumination. From our proposed sketch (Fig. 1), one can observe the

This journal is © The Royal Society of Chemistry 2017
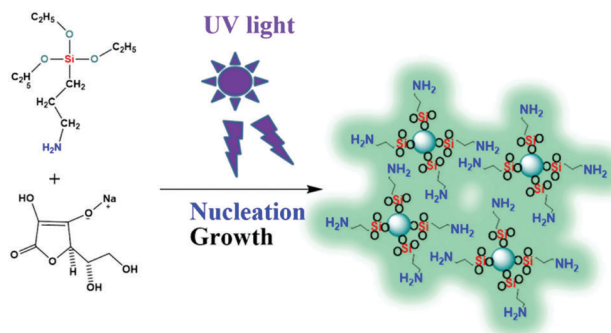
J. Mater. Chem. C, 2017, 5, 1816–1825 | 1817

Fig. 1 General sketch for the synthesis of the surface-modified Si QDs.

growth of the Si QDs and their composition by STEM (Fig. 2a and b) and XPS spectroscopy (Fig. 2c and Fig. S1, ESI†). Specifically, we can examine the Si QDs obtained after 90 min UV illumination (Si QD-90) together with 30 (Si QD-30) and 60 (Si QD-30) min (Fig. S1, ESI†) illumination. Due to the protected and controlled surface environment, Si QDs were monodispersed, having very small nanocrystal sizes ($\sim$2 nm) with a spherical shape, as imaged by STEM and HR-TEM (Fig. 2a and b). The HR-TEM image (Fig. 2a) also displays the high crystallinity of the Si QD-90 and lattice fringes with 0.30 nm interplanar spacing, which is consistent with the (111) plane of diamond Si. From the STEM picture, the available SiO_2 cover on the Si QDs is noticeable.

However, this cover obstructs the easy imaging of the Si QDs. Noticeably, the total reduction procedure is quite fast and can be completed in a short reaction time under room-temperature conditions. The process was scaled up to about 10 g very easily by using a proper amount of precursors. Analysis of the Si QDs by UV absorption (Fig. S2, ESI†) showed their size selective absorption. Under visible light (Fig. 2d), the solution was yellowish-brown but showed a bright green-cyan emission under UV light (Fig. 2e). Additionally, the fluorescence emission measurements (Fig. 2f) for Si QD-90, Si QD-30 and Si QD-60 (Fig. S3, ESI†) were conducted. The results of the elemental composition detected by XPS are shown in Fig. 2c, illustrating the presence of C, Si, N, O and Na. Visual examination of the Si QD-90 solution under visible and UV light unveiled a bright green-cyan emission, which could be used for different applications, as shown in Fig. 2d and e. The uninverted STEM images revealed that there was no agglomeration observed for the Si QDs, but an intense silica environment was detected (Fig. S4, ESI†). The HR-TEM results revealed that the Si QDs were composed of a crystalline silicon core. Also, a silica shell is available, which carries the aminopropyl and –OH groups, thus facilitating water solubility and the possible attachment onto diverse surface functional groups, as detected by XPS spectroscopy (Fig. S5, ESI†). The NMR results (Fig. S6, ESI†) reveal the differences between the starting precursor and the obtained Si QDs surfaces. At the beginning, –OCH_2CH_3 groups are highly visible at 1.12 ppm and 3.54 ppm, respectively.
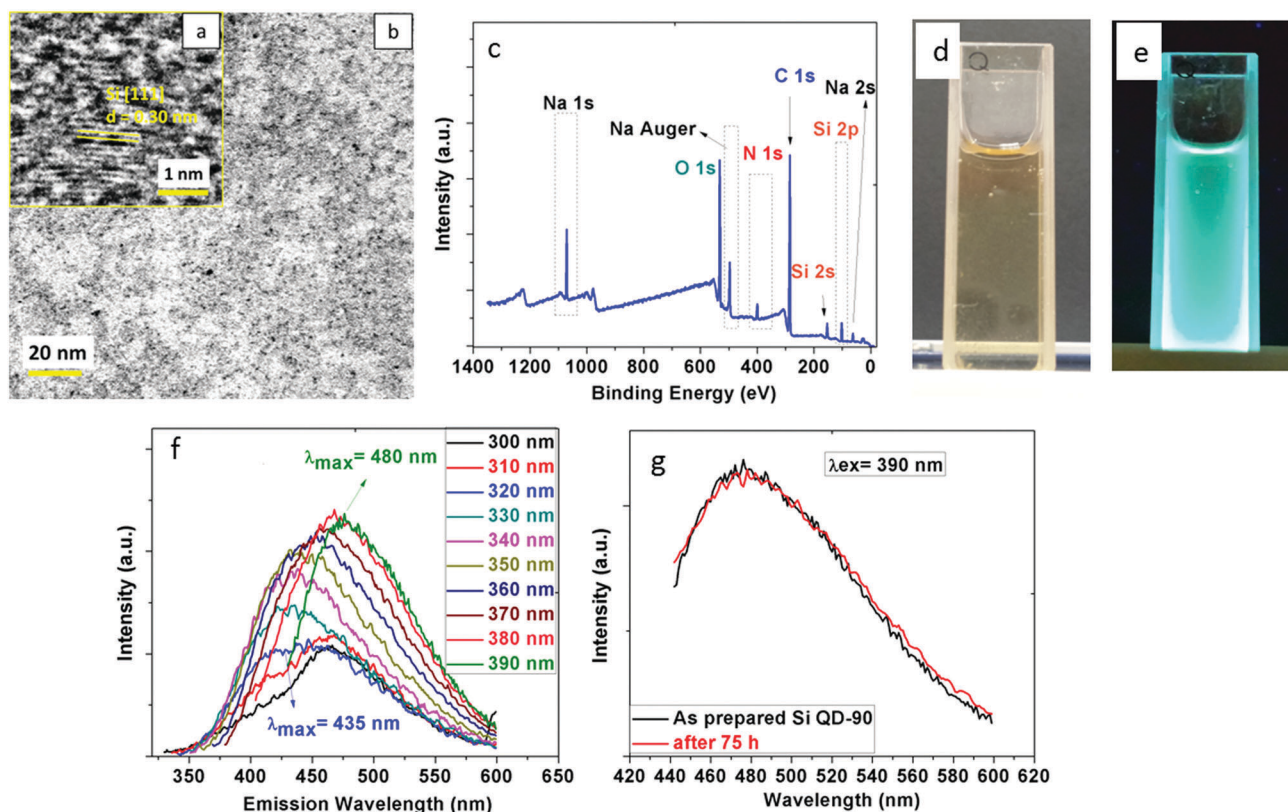

Fig. 2 (a) Representative HR-TEM image for the single Si QD-90 with [111] fringe. (b) Representative TEM image for the Si QD-90. (c) XPS spectrum of the SiQD-90. (d) Visual picture of Si QD-90 solution under visible light. (e) Visual picture of Si QD-90 solution under UV light. (e) PL emissions of the Si QD-90 with different excitation wavelengths. (f) PL of the as-prepared Si QD-90 solution and after 75 hours.

These groups then vanish due to the sol–gel reactions, leaving only the functional –CH$_2$CH$_2$CH$_2$NH$_2$ groups on the Si QDs surfaces. The value of the –NH$_2$ peak is shifted from 1.27 to 1.20 and in addition to that, the values of the carbon-connected protons are shifted, starting (from nitrogen to silicon): 2.58 ppm, 1.52 ppm and 0.58 ppm shifted to 2.81 ppm, 1.62 ppm and 0.57 ppm, respectively. The visible light emission of the Si QDs arises from quantum confinement due to the size of the Si nanostructures (Fig. 2d and e).[16,17] It is prominent that silicon exhibits a weak PL as well as a long exciton-hole recombination time, transforming it into a material that is hard to prepare in huge amounts with monodispersity and uniformity.[18–21] Interestingly, evolution of the Si QDs can be observed by the high-resolution XPS peak shift of the Si 2p, as presented in Fig. S5 (ESI†). A continuous evolution and shift towards lower energy, which possibly provides proof for the increase in the Si QDs formation, is seen. Deconvolution of the Si 2p peaks can also be seen in Fig. S5 (ESI†). The peak maxima shifts from 102.3 eV (30 min) to 102.1 eV (60 min) and then 101.8 eV (90 min), respectively, for the corresponding UV exposure times. Additionally, the high-resolution XPS peaks of the N 1s for the fluorescent probes (Fig. S5, ESI†) showed that there is a constant increase in the peak intensity. Together with a remarkable increase in the region of 400–402 eV. The O 1s high-resolution XPS peaks also facilitate the investigation of the Si QDs evolution (not shown). Even though the different sources for the visible emission are debated in the literature for the Si QDs, the actual origin is still under discussion.[22–25] As shown in Fig. 2d–f and Fig. S3 (ESI†), the Si QDs showed a visible emission between 425 and 500 nm with different excitation wavelengths between 300 and 400 nm, respectively. The results show that the emission maxima corresponding to the λ_{ex} = 390 nm decrease (λ_{em}(30) = 497 nm, λ_{em}(60) = 484 nm, λ_{em}(90) = 480 nm) constantly, which can be attributed to the QD emission peaks changing with the formation and growth steps with the varying surface environment. The excitation wavelength was increased 10 nm in every additional experiment. The PL results showed that after 30 min treatment, the intensity of the corresponding PL peak was almost 5 times lower than the latest measurement. For the 60 and 90 min treatments, almost similar results were obtained. The emission intensities increased stepwise, and generally 400 nm excitation gave the highest corresponding emission peak. If there are no additional reactant preventing the Si QDs formation, then the synthesized QDs can be obtained with the same characteristics. Temperature or high reactant concentrations can cause a variation in the fluorescence emission, also revealed in the literature.[19–21] The results showed that, due to the sol–gel condensation, the Si QDs precipitate within 2–3 days as spherical nanoparticles within a protective layer if they are fabricated under room-temperature conditions. Still, the measurements (Fig. 2g) show that Si QD-90 maintained its visible light emission stability for up to 75 h. According to the PL spectrum analysis (Fig. S7, ESI†), there are 2 components of the Si QDs visible emission that can be detected by the deconvoluted spectra. Observations reveal that in the low excitation wavelengths, a generally broad and unsymmetric PL peak shape is seen, revealing that the possible multi-unsymmetric PL peaks

could be fitted into two peaks, with the first one centred around the emission mechanism. Analysis showed one at 425 nm (2.91 eV) and another positioned at 515 nm (2.50 eV) (Fig. S7, ESI†). According to the literature,[21] we concluded that the lower energy peak possibly originates from surface defects of the Si QDs, which can be affected by the environmental parameters. Additionally a latter peak, which is positioned at higher energy possibly originates from exciton radiative recombination at the core-related levels together with the surface effects.[26] Generally, when the excitation wavelength is increased, a higher emission intensity with better Gaussian morphology at the peaks was observed as an interesting trend. Since silicon structures generally display a large number of dangling bonds, these features can cause surface defects and cause an alteration in the emission intensity. Due to the chemical and highly reactive nature of the precursor, a thin SiO$_2$ layer present on the Si QDs provides a relatively static surface state. Oxygen can also be a very powerful candidate to stabilize the Si QDs surface. XPS analysis showed that the N 1s peak increased its intensity remarkably with the increased illumination times. High-resolution N 1s peaks (Fig. S5, ESI†) revealed an unsymmetric peak shape, with the more energetic part becoming more visible at 398.9 eV and 400.7 eV, respectively. Since fabricated Si QDs carry –NH$_2$ groups on their surface, together with other alkoxy and hydroxyl groups, they are capable of attaching to the different functional surfaces for utilization in sensing applications. From this viewpoint, a proper bonding of the as-prepared Si QDs with a green and facile attachment method onto common polymeric surfaces is essential. There are different routes for the surface modification of the electrospun polymer surfaces for the widely utilized cellulose acetate,[27,28] polyester,[29] Nylon 6,6[30] and polycaprolactone (PCL)[31] materials as one of the most rapidly emerging areas for the different applications. These polymeric structures behave mostly hydrophilically, transforming their electrospun nanofibre utilization to a limited degree because of their durability and stability drawbacks. Therefore, the facile modification of these molecules is of great interest, prompting various studies involving homogeneous substitution or the reaction with hydroxyl, carboxyl or amino groups available on these materials. Some relatively common modification methods for nanostructured materials include the sol–gel method,[32,33] graft polymerization,[34,35] plasma treatment[36,37] and impregnation techniques.[35,36] From the chemical interaction approach, esterification via –OH groups is the most common process to prepare surface-tailored polymeric structures. Additionally, carboxylic addition or amine reaction can also provide further functionalization when the proper conditions are utilized. Since alkoxy groups on the precursor silane during this fabrication method are prone to sol–gel chemistry mediated attacks, hydrolysis/condensation reactions are facilitated, and once alkoxysilane reacts with the proper functional groups,[32] surface decoration by these as-synthesized Si QDs is possible. Here, we successfully electrospun bead-free and uniform Nylon 6,6 nanofibres ((Fig. 3a1–a3) from 10% (w/v) polymer solutions with an average fibre diameter of 90 ± 20 nm (Fig. S8, ESI†). Afterwards, the as-synthesized Si QDs (Si QD-90) were deposited onto this flexible polymeric nanofibrous mat, and it was
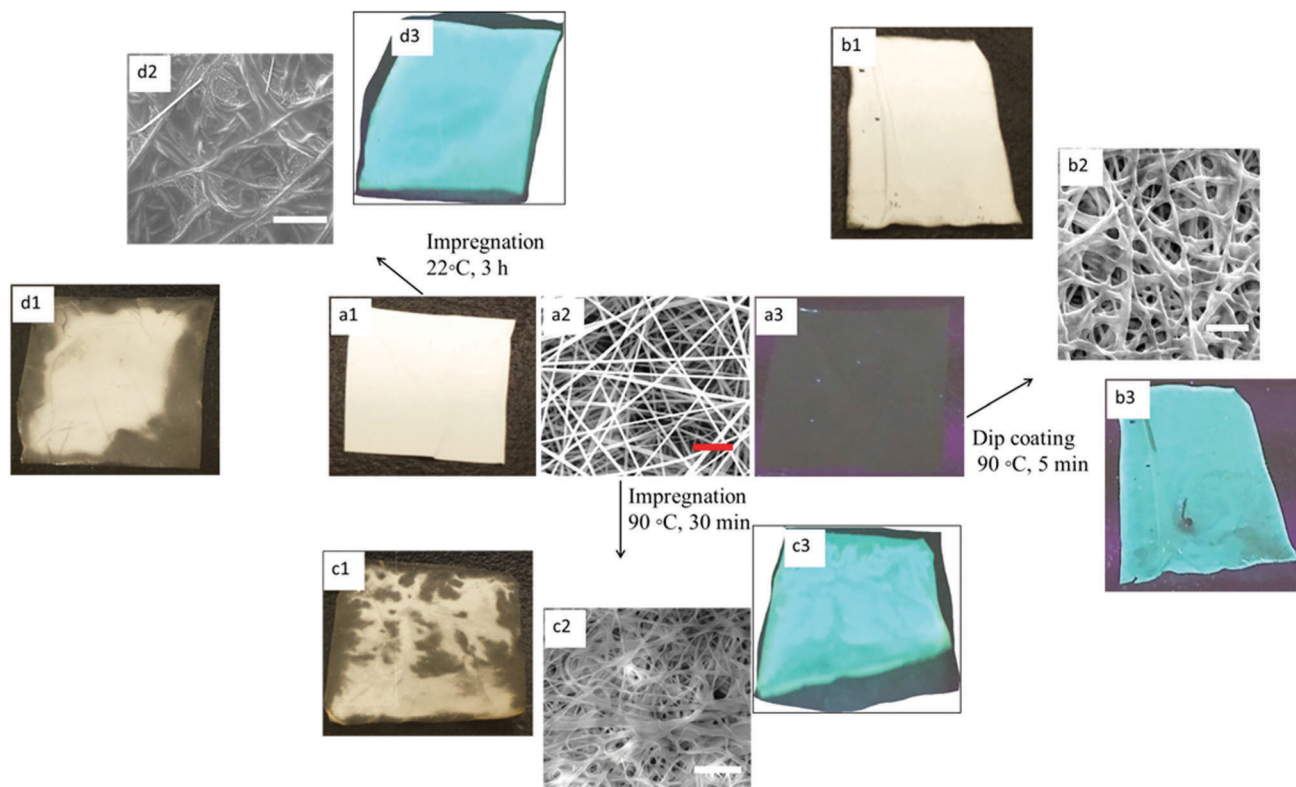
This journal is © The Royal Society of Chemistry 2017

J. Mater. Chem. C, 2017, 5, 1816–1825 | 1819

Fig. 3   (a1) Electrospun Nylon 6,6-NF under visible light. (a2) Representative SEM image of the Nylon 6,6-NF (scale bar = 1 µm). (a3) Nylon 6,6-NF under UV light. (b1) Si QD-90-decorated Nylon 6,6-NF by dip coating under visible light. (b2) Representative SEM image of the Si QD-90-decorated Nylon 6,6-NF by dip coating (scale bar = 1 µm). (b3) Dip-coated Si QD-90-decorated Nylon 6,6-NF under UV light. (c1) Si QD-90-decorated Nylon 6,6-NF by the impregnation method and at 90 °C, 30 min drying, under visible light. (c2) Representative SEM image of the Si QD-90-decorated Nylon 6,6-NF by the impregnation method and at 90 °C, 30 min drying (scale bar = 2 µm). (c3) Impregnation method, Si QD-90-decorated and at 90 °C, 30 min dried Nylon 6,6-NF under UV light. (d1) Impregnation method, Si QD-90-decorated air (22 °C) 3 h dried Nylon 6,6-NF under visible light. (d2) Representative SEM image of the impregnation method, Si QD-90-decorated Nylon 6,6-NF (scale bar = 2 µm). (d3) Impregnation method, Si QD-90-decorated and air (22 °C) 3 h dried Nylon 6,6-NF under UV light.

observed that the fibrous structure was kept after the dip-coating process (Fig. 3b1–b3). During the surface modification, the impregnation method and dip-coating processes were applied separately and analyzed thoroughly to detect the best Si QD deposition technique for deposit onto the electrospun mats. The details of the whole coating processes are given in the experimental part. Since the Si QDs have functional –OH, –NH$_2$ and alkoxy groups arising from the propagated sol–gel reaction, when the dip-coating process is applied, the Nylon 6,6-NF surface (N–H and C=O) structure interacts with the functional groups present in the Si QD-90 colloidal solution. SEM image of the Si QD-90-decorated nanofibres showed that the smooth morphology of the Nylon 6,6-NF (Fig. 3a1–a3) was slightly disturbed and became slightly rougher due to the Si QD-90 decoration (Fig. 3b1–b3). For comparison, an impregnation method for the Si QDs deposition was conducted with the prepared 200 µL Si QD-90 solution.

After dropping the Si QD-90 solution onto the Nylon 6,6 nanofibrous mats, the drying procedure was varied to define the best way of decoration. In the first drying method tested for the impregnation route, Si QD-90 impregnated nanofibrous 2 × 2 cm mats were cured at 90 °C for 30 min (Fig. 3c1–c3)

and labelled as 1. Other nanofibrous mats were dried under room-temperature conditions (2 × 2 cm dimensions, 22 °C, 45% humidity, 3 h) and labelled as 2 (Fig. 3d1–d3). Morphological and visual observations were conducted by SEM as shown in every corresponding decorated nanofibrous mat. The impregnation method with two separate drying processes provided an inhomogeneous deposition of the Si QD-90, possibly arising from SiO$_2$ pools covering the surface of the Nylon 6,6-NF, leading to local optical problems (Fig. 3c2 and d2) for the nanofibrous mats. At 90 °C and 30 min drying, the SEM investigation (Fig. 3c2) revealed that the heating and curing procedure under these conditions transformed the nanofibrous mats in an almost similar way to that for the dip-coated nanofibrous mats (Fig. 3b2). Only the roughness increases, and the morphological differences observable are possibly due to the water absorption on the Si QD-90. On the contrary, the room temperature (22 °C, 45% humidity, 3 h) dried method yielded compact and fully surface-covered nanofibrous mats (Fig. 3d2), which actually effectively veiled the surface of the Nylon 6,6-NF and transformed the mat into another new nanostructure. Here, possibly, completion of the sol–gel reactions was not finalized and instead of surface interaction, components of the Si QD-90 colloidal solution reacted with each other and

formed a dense SiO_2 layer over the top. Under UV illumination, the fluorescent feature of the impregnated fibres are perfectly suitable, whatever drying procedure is used, but optically, morphologically and elastically, the results are not promising. In addition to this, when dip-coated Si QD-90 decoration of the Nylon 6,6-NF was conducted (Fig. 3a1–a3), preservation of the morphology was seen before and after Si QD-90 decoration. Examination under UV light without and with Si QD-90 showed the visible light emitting characteristics of the nanofibrous mats. The homogeneous photoluminescence characteristics and better optical coverage and indeed almost no morphological variations supported the idea of a higher compatibility for the dip-coating method. The Si QD-90-decorated Nylon 6,6-NF mat was illuminated with UV light, while the green emitting nanofibrous mat was detected easily. For further analysis of the dip-coating process, the deposited Si QD-90 layer was examined by TEM (Fig. 4a), XPS (Fig. 4b) and STEM-HDAAF-EDX mapping (Fig. 4c). Since the Si QD-90 layer attached to the Nylon 6,6 acts as a fluorescence coating, one can detect the coated region on the nanofibre surface, as seen in the TEM imaging (Fig. 4a). XPS analysis revealed (Fig. 4b) Si 2p peaks arising from the Si QD-90 formulation. Since sol–gel chemistry provides the proper attachment onto the Nylon 6,6-NF, the mats interact with these semi-polymeric alkoxysilane species at a molecular level to form a protective and fluorescent layer. STEM-HDAAF-EDX mapping (Fig. 4c) of N, O and Si was performed and clearly revealed the presence of a Si QDs coating. The brighter fields showed the denser atomic availability in the STEM mapping. In the last overlapped STEM image, blue represents nitrogen, green represents oxygen and red represents silicon atoms. If we compare the impregnation and dip-coating processes, an excessive Si content can be speculated on and was detected by the EDX spectra (Fig. S9, ESI†) and quantitative analysis. The results interestingly showed that the room-temperature dried impregnated nanofibrous mats (Si = 20.5%) had almost 2 times more Si content than the 90 °C, 30 min dried impregnated mats (Si = 10.1%). This is possibly due to the extreme number of different silicon species occurring in uncontrolled and uncompleted sol–gel reactions. Strikingly, the dip-coated Nylon 6,6-NF contained only 8.4% Si, which is the lowest amount among the deposition techniques. By lowering the withdrawal speed, this level could possibly be decreased.[38,39] EDX mapping analysis of the dip-coated sample (Fig. 5) clearly shows the available atomic entities together with the Na content, which comes from the reducing agent. The mapping results clearly show the homogeneous distribution of the Si QD-90 on the Nylon 6,6-NF. FT-IR investigation (Fig. S10a, ESI†) also showed that a Si–O peak
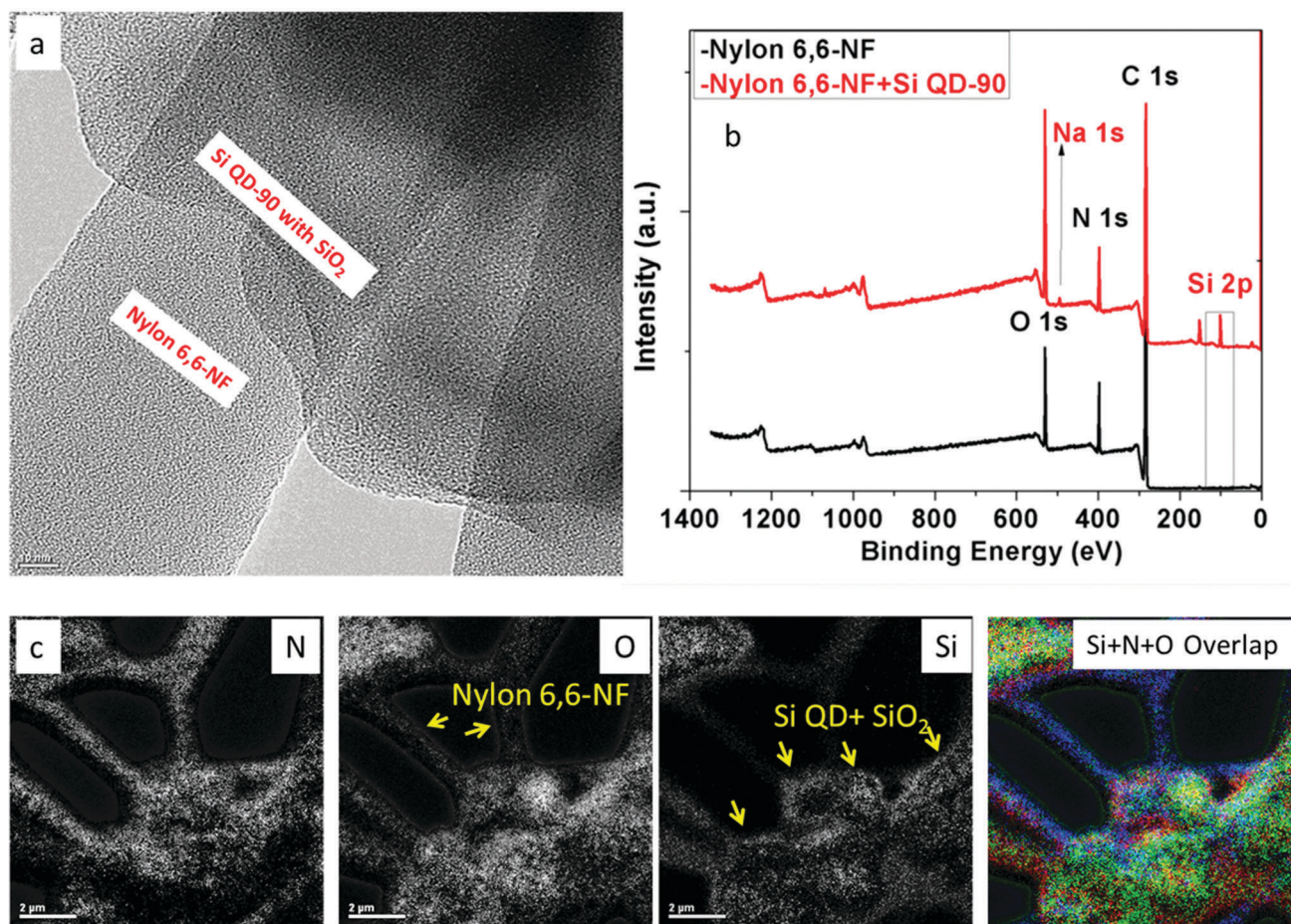

Fig. 4 (a) Representative TEM image of the Si QD-90 coated Nylon 6,6-NF (b) XPS spectra of the Nylon 6,6-NF and Si QD-90 coated Nylon 6,6-NF (c) STEM-HAADF-EDX atomic mapping of the Si QD-90 coated Nylon 6,6-NF (blue = nitrogen, green = oxygen, red = silicon).
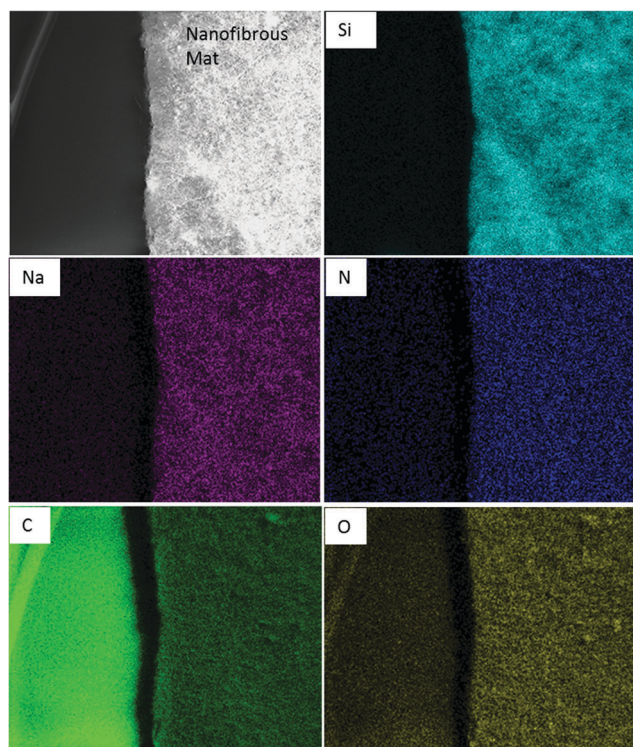
This journal is © The Royal Society of Chemistry 2017

J. Mater. Chem. C, 2017, 5, 1816–1825 | 1821

Fig. 5 EDX atomic mapping for the dip-coated Si QD-90 decoration on the Nylon 6,6-NF mat.

appears at 980 cm^{-1} in addition to the other Nylon 6,6-NF peaks, where the N–H peak appears at 3310 cm^{-1} and the unsymmetrical C=O peak is seen at 1642 cm^{-1} for the amide structure.[40] When compared, the dip-coated sample showed a remarkably lower intensity for the Si–O peaks, and, as expected, the air-dried sample had the higher intensity, which confirms the higher quantity of Si QDs decoration. Thermal analysis (Fig. S10b, ESI†) also supported the findings about the higher loading by the impregnation method. The TGA results showed that Nylon 6,6-NF starts to decompose at around 400 °C[41] and this ends at 510 °C, losing almost all of its components (97%), but when it is decorated with Si QD-90, due to the water and other volatile components, the structures gave three different decomposition regions. First, the impregnated and dip-coated samples appear to have the same decomposition characteristics, but due to the different amount of decoration, the weight% loss amounts are different. First, the weight losses start in the 150–170 °C range, and possibly belong to water and other surface adsorbed volatile entities. Up till 180 °C, an 8% loss from the impregnated samples was observed. This level was 4% for the dip-coated sample. After that, a second decomposition starts at 340 °C till 410 °C, while the third loss continues until 520 °C. The air-dried sample loses 86% until 800 °C, and this value is 90% for the 90 °C dried sample. The dip-coated sample loses 94% weight and possibly losses SiO$_2$, as other samples also behave similarly. Consequently, the extreme loading and inhomogeneity were also confirmed by thermal analysis. Fig. 6a shows the Si QD-90 decoration method for the Nylon 6,6,-NF. Although in the literature. TNT vapour[42] is used with some

other techniques[43,44] for the detection of TNT molecules, since TNT is an important and water-soluble pollutant, we focused on aqueous detection. Some studies[44] focus on the SERS detection of the TNT, but TNT is a water-soluble molecule and its detection in soil-based environments is vital. By investigating the quenching efficiencies (Fig. 6b) of the Si QDs with different concentrations of TNT, we were able to detect the Stern–Volmer plot (Fig. S11, ESI†), and the fitting results showed that the quenching relationship was $y = 0.51$ [TNT] $+ 0.92$, and there is a direct relationship between the quenching constant and the concentration of the trinitro group linked to the aromatic ring, which results from the strong electron-withdrawing effect of the nitro group. Fig. 6c represents the colorimetric sensing mechanism of the as-prepared Si QD-90 for TNT. It is known that QD fluorescence is very sensitive to external parameters and concentration. After the dip coating, the visible emission peak of the Nylon 6,6/Si QD-NF were shifted slightly from 482 nm to 484 nm as a result of stacking or light re-adsorption, which can also effect the FRET feature.

Surprisingly, the emission peak of the Si QD-90-decorated nanofibrous mat did not show any remarkable deviation from the prepared mother solution. Literature showed that if FRET is to happen in solid nanomaterials with embedded QDs, a higher quantity of shorter wavelength emitters has to be introduced due to the energy transfer compensation to longer wavelength emitters.[45–48] Since light-controlled sol–gel reactions provide very active chemical functionalities for the fabrication of Si QD-90, decoration onto the flexible Nylon 6,6 mats is easier. It is known that, after the coating/decoration processes, the drying process for the electrospun polymeric nanostructure is remarkably faster. This is due to the solvent leaving the high-surface-area-to-volume fibre surfaces very rapidly to equilibrate the thermodynamic heat transfer. This phenomenon can also lead to physical and mechanical variations on the electrospun nanofibres, but the SEM investigation showed no remarkable change in our case. It is widely known that TNT can selectively interact with primary amines by donor–acceptor chemistry (Fig. 6c).[49] When interaction occurs, an electron transfer from the primary amine to the aromatic ring facilitated by the side groups takes place. We have already illustrated the amine–TNT complex formation in Fig. 6c. Formation of the complex can be visualized by UV spectroscopy, but a decrease in fluorescence response can be more effective. Since Si QD-90 carry primary amino groups on the surface, the addition of different concentrations decreases the fluorescence intensity, which can be observed and plotted by the Stern–Volmer approach. For quantification of the TNT analyte, the Stern–Volmer equation was utilized as follows:

$$I_0/I = 1 + KS_V[A] \tag{1}$$

where I_0 is the initial fluorescence intensity without the analyte, I is the fluorescence intensities of the analyte responses with different concentrations, KS_V is the quenching constant and [A] is the analyte concentration, which we explained earlier. Fig. 6d–g shows the visual colour change of the Si QD-90-decorated Nylon 6,6-NF mat after TNT quenching. Visual colorimetric observation of the TNT was performed *via* the PL technique for different

1822 | *J. Mater. Chem. C*, 2017, **5**, 1816–1825

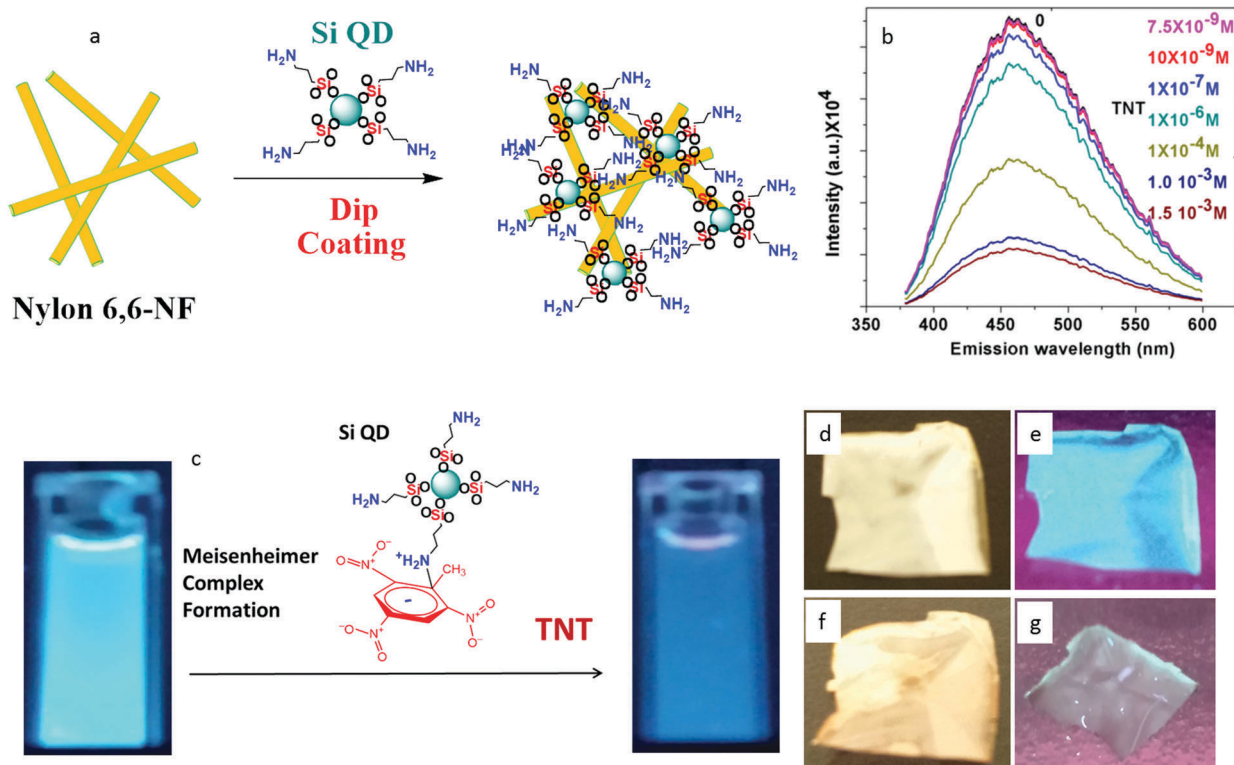This journal is © The Royal Society of Chemistry 2017

Fig. 6 (a) Si QD-90-decorated Nylon 6,6-NF fabrication by dip coating. (b) Quenching efficiencies of the Si QD-90 with different concentrations. (c) Formation of the Meisenheimer complex with Si QD-90 for 1 mM solution under UV light. (d) Si QD-90-decorated Nylon 6,6-NF under visible light. (e) Si QD-90-decorated Nylon 6,6-NF under UV light. (f) Si QD-90-decorated Nylon 6,6-NF treated with 7.5 nM TNT under visible light. (g) Si QD-90-decorated Nylon 6,6-NF treated with 7.5 nM TNT under UV light.

concentrations of TNT from 1.5 mM to 7.5 nM. It is highly visible that the sensing performance of the Si QD-90 is easily identifiable (Fig. 6f–g) with UV light (λ_{ext}: 352 nm) by the naked eye, in the TNT solutions at selected concentrations. The origin of this colour is the Meisenheimer complex (Fig. 6c), requiring the availability of –NH$_2$ groups on the fluorescent nanostructures.[50–52] Since the aromatic structure is highly stable, the reaction and/or response times of the Si QD-90 was found within 10–30 s after the TNT exposure by dropping. Notably, a colour change was observable on dried nanofibrous mats, indicating their rapid response character. PL quenching experiments were conducted up till 7.5 nM (Fig. 6d–g), which transformed the nanofibrous mat surface to a slightly wine-red colour. To check the solvent effect for detection, the treatments were used without TNT, and no change was observed as expected. 1 mM and 1.5 mM TNT levels were also detected. Investigations on the nanofibrous mat after the subsequent treatment with TNT showed (Fig. S12a–c, ESI†) that the defined previous morphology of the fibrous structure was the same and that higher analyte concentrations did not cause variations in the fibre structure. Interestingly, when the dip-coated nanofibrous mats were stored in highly acidic (pH = 2.3) and highly basic (pH = 12.6) solutions over a 1 h period, there was no change in visible emission, stressing the protective feature of the SiO$_2$ layer around the Si QD-90 (Fig. S13, ESI†). As one of the general ceramic forming components, SiO$_2$ plays the role of Si QD-90 surface protection and helps

to maintain the fluorescence intensity, even in these extreme conditions. The stability of the as-prepared Si QDs was also tested (Fig. 2g). Basically, according to this process, Si QDs fabrication involves a sol–gel system, leading to the formation of the SiO$_2$ structures when stored. Still, the Si QDs solution maintains its fluorescence intensity and spectral position for 75 h (Fig. 2g). After 75 h, due to the extreme and uncontrolled hydrolysis and condensation reactions, Si QDs emission starts to deviate from its original properties. The Si QDs precipitate within the SiO$_2$ nanoparticles, and then, even though they still emit green light, solid nanocomposite silica structures are obtained, as shown in Fig. S14 (ESI†). We also evaluated the specificity of the probe towards TNT by using PNP and toluene as other aromatic analytes. As expected, the results highlighted that the mono-nitro compound (4-nitrophenol (PNP)) can slightly decrease the fluorescence intensity as shown (Fig. S15a–b, ESI†) but toluene showed no decrease in intensity. These results show that the as-prepared Si QDs are superior structurally, and from a surface functionality perspective, when compared to the previous nanoparticle/QD preparations, for which their detection levels were at the μmolar level.[53,54] Even though TNT vapour utilization may vary the conditions, it should be highlighted that our results are relatively better than in previous experiments, where the detection limits were in the μmolar level.[55–57]

Consequently, we have shown that, visible light emitting Si QDs can be fabricated by a light-controlled procedure and

This journal is © The Royal Society of Chemistry 2017

J. Mater. Chem. C, 2017, 5, 1816–1825 | 1823

can be decorated onto electrospun, nanofibrous and flexible Nylon 6,6, mats to transform them into colorimetric sensors *via* their quenchable visible emission properties. Due to the suitable chemical functionalities available on the surface of the Si QDs, Nylon 6,6 nanofibrous mats were coated in nm thickness and they showed selective efficiency for the determination of TNT, as our analytical investigations revealed.

Conclusions

We developed a colorimetric TNT sensor by the decoration of Si QDs onto nanofibrous Nylon 6,6, mats *via* a dip-coating process. Light-controlled fabrication of the Si QDs facilitated the TNT sensing procedure, since $-NH_2$ groups available on the Si QDs surface play an important role. For an optimal Si QDs-decoration process onto nanofibrous Nylon 6,6, mats, we also investigated the impregnation and dip-coating processes separately to detect the proper conditions. Molecular interaction between the aromatic TNT ring and $-NH_2$ carrying Si QDs, which were decorated onto the nanofibrous Nylon 6,6, mats, allowed us to define the low amounts of analyte, as revealed by the results. The examinations also convinced us that the fabricated surface-tailored Si QDs may be utilized to design other colorimetric sensor structures for the preparation of cheap and rapid detectors for different applications.

Acknowledgements

Notes and references

1 E. Secret, L. Camille, J. K. Stefan, U. Amanda, C. Cozzan and J. S. Andrew, *Langmuir*, 2016, **32**, 1166.

2 X. Li, Y. He and M. T. Swihart, *Langmuir*, 2004, **20**, 4720.

3 M. H. Nayfeh, US 20120195977 A1, 2012.

4 F. E. Kruis, H. Fissan and A. Peled, *J. Aerosol Sci.*, 1998, **29**, 511.

5 V. G. Pol, D. N. Srivastava, O. Palchik, V. Palchik, M. A. Slifkin, A. M. Weiss and A. Gedanken, *Langmuir*, 2002, **18**, 3352.

6 J. Liang, X. Li, Y. Zhu, C. Guo and Y. Qian, *Nano Res.*, 2015, **8**, 1497.

7 R. D. Tilley, J. H. Warner, K. Yamamoto, I. Matsui and H. Fujimori, *Chem. Commun.*, 2005, 1833.

8 A. G. Cullis and L. T. Canham, *Nature*, 1991, **353**, 335.

9 K. Dohnalová, T. Gregorkiewicz and K. Kůsová, *J. Phys.: Condens. Matter*, 2014, **26**, 173201.

10 G. Ledoux, J. Gong, F. Huisken, O. Guillois and C. Reynaud, *Appl. Phys. Lett.*, 2002, **80**, 4834.

11 A. R. Jose, U. Sivasankaran, S. Menona and K. G. Kumar, *Anal. Methods*, 2016, **8**, 5701.

12 S. Chinnathambi, S. Chen, S. Ganesan and N. Hanagata, *Adv. Healthcare Mater.*, 2014, **3**, 10.

13 L. Persano, A. Camposeo, C. Tekmen and D. Pisignano, *Macromol. Mater. Eng.*, 2013, **298**, 504.

14 S. Ramakrishna, K. Fujihara, W.-E. Teo, T.-C. Lim and Z. Ma, *An introduction to electrospinning and nanofibers*, World Scientific, 2005.

15 J. H. Wendorff, S. Agarwal and A. Greiner, *Electrospinning: materials, processing, and applications*, John Wiley & Sons, 2012.

16 S. Yang, W. Li, B. Cao, H. Zeng and W. Cai, *J. Phys. Chem. C*, 2011, **115**, 21056.

17 K. Linehan and H. Doyle, *Small*, 2014, **10**, 584.

18 M. Dasog, G. B. D. Reyes, L. V. Titova, F. A. Hegmann and J. G. C. Veinot, *ACS Nano*, 2014, **8**, 9636.

19 W. Sun, C. Qian, K. K. Chen and G. A. Ozin, *ChemNanoMat*, 2016, **2**, 842.

20 B. L. Oliva-Chatelain, T. M. Ticich and A. R. Barron, *Nanoscale*, 2016, **8**, 1733.

21 Y. Su, X. Ji and Y. He, *Adv. Mater.*, 2016, **28**, 10567.

22 C. Delerue, G. Allan and M. Lannoo, *Phys. Rev. B: Condens. Matter Mater. Phys.*, 1993, **48**, 11024.

23 D. J. Lockwood, Light Emission in Silicon: From Physics to Devices, *Semiconductors and Semimetals*, Academic Press, 1998, vol. 49.

24 A. A. Ischenko, G. V. Fetisov and L. A. Aslanov, Nanosilicon Properties, Synthesis, Applications, *Methods of Analysis and Control*, CRC Press, 2015.

25 J. D. Holmes, K. J. Ziegler, R. C. Doty, L. E. Pell, K. P. Johnston and B. A. Korgel, *J. Am. Chem. Soc.*, 2001, **123**, 3743.

26 J. Liu, F. Erogbogbo, K. Yong, L. Ye, J. Liu, R. Hu, H. Chen, Y. Hu, Y. Yang, J. Yang, I. Roy, N. A. Karker, M. T. Swihart and N. P. Paras, *ACS Nano*, 2013, 7, 7303.

27 O. Arslan, Z. Aytac and T. Uyar, *ACS Appl. Mater. Interfaces*, 2016, **8**, 19747.

28 A. Senthamizhan, B. Balusamy, A. Celebioglu and T. Uyar, *J. Mater. Chem. A*, 2016, **4**, 2484.

29 F. Kayaci, Z. Aytac and T. Uyar, *J. Hazard. Mater.*, 2013, **261**, 286.

30 F. Kayaci, C. Ozgit-Akgun, N. Biyikli and T. Uyar, *RSC Adv.*, 2013, **3**, 6817.

31 A. Senthamizhan, A. Celebioglu and T. Uyar, *Sci. Rep.*, 2015, **5**, 10403.

32 O. Arslan, E. Arpaç, F. Sayılkan and H. Sayılkan, *J. Mater. Sci.*, 2007, **42**, 2138.

33 A. E. Danks, S. R. Hall and Z. Schnepp, *Mater. Horiz.*, 2016, **3**, 91.

34 A. Bhattacharyaa and B. N. Misra, *Prog. Polym. Sci.*, 2004, **29**, 767.

35 O. Arslan, E. Arpac and H. Sayılkan, *J. Inorg. Organomet. Polym. Mater.*, 2010, **20**, 284.

36 P. K. Chua, J. Y. Chena, L. P. Wanga and N. Huang, *Mater. Sci. Eng., R*, 2002, **36**, 143.

37 S. B. Said, F. Arefi-Khonsari and J. Pulpytel, *Plasma Processes Polym.*, 2016, **13**, 1025.

1824 | *J. Mater. Chem. C*, 2017, **5**, 1816–1825

This journal is © The Royal Society of Chemistry 2017

38 L. Delannoy, N. El Hassan, A. Musi, N. N. Le To, J. M. Krafft and C. Louis, *J. Phys. Chem. B*, 2006, **110**, 22471.

39 H. Choi, S. R. Al-Abed, S. Agarwal and D. D. Dionysiou, *Chem. Mater.*, 2008, **20**, 3649.

40 M. Faustini, B. Louis, P. A. Albouy, M. Kuemmel and D. Grosso, *J. Phys. Chem. C*, 2010, **114**, 7637.

41 F. Kayaci, H. S. Sen, E. Durgun and T. Uyar, *J. Appl. Polym. Sci.*, 2015, **132**, 41941.

42 Q. Liu, K. Qiu, S. He, H. Liu, Z. Liu, Y. Honga and S. Fua, *Analyst*, 2016, **141**, 4018.

43 H. Zhou, Z. Zhang, C. Jiang, G. Guan, K. Zhang, Q. Mei, R. Liu and S. Wang, *Anal. Chem.*, 2011, **83**, 6913.

44 H. Liu, D. Lin, Y. Sun, L. Yang and J. Liu, *Chem. – Eur. J.*, 2013, **19**, 8789.

45 O. Arslan, A. P. Singh, L. Belkoura and S. Mathur, *J. Mater. Res.*, 2013, **14**, 1947.

46 O. Arslan, L. Belkoura and S. Mathur, *J. Mater. Chem. C*, 2015, **3**, 11965.

47 A. Senthamizhan, A. Celebioglu and T. Uyar, *J. Mater. Chem. A*, 2014, **2**, 12717.

48 A. Senthamizhan, A. Celebioglu, S. Bayir, M. Gorur, E. Doganci, F. Yilmaz and T. Uyar, *ACS Appl. Mater. Interfaces*, 2015, **7**, 21038.

49 A. Senthamizhan, A. Celebioglu and T. Uyar, *Chem. Commun.*, 2015, **51**, 5590.

50 X. Sun, Y. Wang and Y. Lei, *Chem. Soc. Rev.*, 2015, **44**, 8019.

51 R. Ban, F. Zhenga and J. Zhang, *Anal. Methods*, 2015, **7**, 1732.

52 Y. Salinas, R. Martínez-Máñez, M. D. Marcos, F. Sancenón, A. M. Costero, M. Parra and S. Gil, *Chem. Soc. Rev.*, 2012, **41**, 1261.

53 W. J. Peveler, A. Roldan, N. Hollingsworth, M. J. Porter and I. P. Parkin, *ACS Nano*, 2016, **10**, 1139.

54 S. Hughes, S. S. R. Dasary, S. Begum, N. Williams and H. Yu, *Sensing and Bio-Sensing Research*, 2015, **5**, 37.

55 F. Zang, K. Gerasopoulos, X. Z. Fan, A. D. Brown, J. N. Culverc and R. Ghodssi, *Chem. Commun.*, 2014, **50**, 12977.

56 G. He, N. Yan, J. Yang, H. Wang, L. Ding, S. Yin and Y. Fang, *Macromolecules*, 2011, **44**, 4759.

57 R. Tu, B. Liu, Z. Wang, D. Gao, F. Wang, Q. Fang and Z. Zhang, *Anal. Chem.*, 2008, **80**, 3458.